Ab Initio Investigation of Ethane Dissociation Using Generalized Transition State Theory

François Lorant* and Françoise Behar

Institut Français du Pétrole, Geology and Geochemistry Research Division, 1-4 avenue de Bois Préau, 92852 Rueil-Malmaison Cedex, France

William A. Goddard, III

Material Simulation Center, Beckman Institute (139-74), California Institute of Technology, Pasadena, California 91125

Yongchun Tang

Petroleum Energy and Environmental Research Center, California Institute of Technology, 20970 Currier Rd, Walnut, California 91789

Received: November 7, 2000; In Final Form: March 29, 2001

The simple carbon−carbon scission of ethane is investigated by performing quantum mechanical calculations. The approach described in this paper was developed to determine dissociation rate constants for both small and large organic molecules, such as *n*-alkanes or alkyl-benzenes, for reasonable ranges of computation time and accuracy. The methodology that we propose is based on generalized transition state theory, where transition states are defined along rate constant profiles and not along potential energy curves. Simulations reported in this paper aim to validate this methodology by examining the dissociation of ethane. Calculations, performed at the DFT B3:LYP 6-31G** theory level, correctly account for the looseness of the transition state as a function of temperature. Dissociation activation parameters obtained by this method are in good agreement with data available in the literature. Despite the assumptions made, the order of magnitude and the specific temperature dependence of rate constants for methyl recombination are also fairly predicted.

1. Introduction

Transition-state theory[1] (TST) is the most practical model for calculating rates of gas-phase elementary reactions. The course of a chemical reaction is determined by a potential-energy function that depends on the coordinates of the N nuclei of the reactant molecules. On the corresponding potential energy surface (a 3N-6 dimension surface in the general case), the minimum-energy path connecting reactants and products defines the reaction coordinate. In the classical TST, the point of maximum potential energy along this coordinate, which is a first-order saddle point on the potential energy surface, corresponds to a transition state (TS) that maintains equilibrium Boltzmann distributions of energy with the reactants. The rate of the reaction is thus given by the product of the TS concentration and the rate constant for its passage over the energy barrier.

Most quantum chemical software packages currently available allow the user to predict absolute rate constants using conventional TST. Knowing the reactants and the products of a reaction, a TS search on the corresponding potential energy surface can be automatically performed (standard searching methods are briefly described in ref 2 and 3). Molecular properties (entropy, free energy, vibrational frequencies, etc.) can then be assigned to the optimized TS structure (although it is not a stable molecule), and activation parameters can be calculated. Beyond the problem of validity of the TS structure, quantitative uncertainties with such an approach mostly result from (i) the level of quantum theory used to calculate the potential energy function and (ii) the difficulty in verifying that the correct frequencies have been assigned to the TS[4].

Guided-TS searches on potential energy surfaces are restricted, however, to chemical processes where conventional TST applies. Reactions like simple bond dissociation and radical recombination usually do not show any energy barrier, and so it can be difficult to locate a TS along their reaction paths. The specific problem of evaluating rate constants for barrierless processes has been discussed by various authors.[5−11] The theoretical treatments of Wardlaw and Marcus[8], based on RRKM theory, have greatly improved our understanding of such reactions.[11] Their "flexible" TST accounted for both the negative temperature dependence of recombination rate constants, as experimentally observed (see references in 8 and 10), and the temperature dependence of TS looseness. Unfortunately, this level of theory is currently limited to processes that involve small molecules and radicals (e.g., recombination of methyl radicals or ethane dissociation). Despite further improvements (see for example discussion in ref 7), the application of flexible TST still requires considerable computational effort, and the prediction of rate constants for scission of simple bonds within larger reactant molecules using quantum chemical approaches remains challenging.

Our aim is to propose a methodology that can be used to determine absolute rate constants for the direct dissociation of both small and large organic molecules. This methodology should not require specific programming, since it makes use of current quantum chemistry tools, through which large molecular systems may be modeled with a reasonable level of accuracy and at reasonable computational cost. However, to limit the number of ab initio calculations, only one path across the

* Corresponding author. E-mail: francois.lorant@ifp.fr.

10.1021/jp004094a CCC: $20.00
Published on Web 07/26/2001

potential energy surface will be considered. Because of this restriction, uncertainties associated with calculated rate constants may be high in some cases.

To validate this approach, we first attempted to evaluate activation parameters for the direct dissociation of ethane into two methyl radicals. Ab initio investigations of this reaction constitute the topic of this paper. QM results (i.e., geometries, frequencies, TS localization along the reaction coordinate, and activation parameters) are reported and compared to experimental data and theoretical models available in the literature.

2. Calculation Methodology

All quantum mechanics simulations were performed using JAGUAR[12] software (version 4.0, release 13). Self-consistent field energies (SCFE) were calculated at the B3:LYP density functional theory level[13] (DFT B3:LYP) using the 6-31G** basis set. Reactant molecules were calculated in a closed-shell system, and reaction products and excited states were simulated in an open shell system.

2.1. Singlet State Potential Energy Curve and Vibrational Frequencies. Intermediate geometries along the reaction coordinate, i.e., one carbon−carbon bond distance, were selected and optimized by starting with a very large extension coefficient ($r_{CC}/r^{e}_{CC} \approx 13$, where r_{CC} is the C−C bond distance of the unstable structure and r^{e}_{CC} that of the stable molecule), to the equilibrium structure at $r_{CC}/r^{e}_{CC} = 1$. In all cases, we assumed both methyl groups have a face-to-face orientation, perpendicular to the C−C axis. According to recent work[10], this hypothesis appears to be reasonable in the case of short C−C distances ($r_{CC} < 4.5$ Å) but may be less appropriate for larger bond distances.

Angles, bond distances (except the reaction coordinate), and wave functions for each optimized structure were introduced to initiate energy minimization of the closest geometry of lower energy along the reaction pathway. Orbital backward-projection from step to step was a critical point in our methodology. This approach accelerated geometry optimizations and prevented local convergence of wave functions that may result in erratic fits to potential energy curves. To ensure that the direction of optimization yielded minimum energy structures, each orbital projection was performed after refinement of the Hessian.[2] Vibrational frequencies were computed from the improved force constants matrix.

2.2. Transition State Definition and Location. For chemical processes that have a potential energy maximum on their reaction path, it is convenient to make the approximation that TS are fixed structures which can be searched on SCFE surfaces. However, as mentioned previously, it is well-known that this restricted TST fails to account for reactions which have potential energy profiles in the shape of a Morse function. Strictly speaking, TS should actually be localized on energy surfaces that include enthalpy and entropy contributions. Hence, the key assumption of our work was that dissociation reactions can be satisfactorily described by the generalized TST[3], which is based on the variation of free energy ($\Delta G^{\ddagger}$) along the reaction coordinate rather than the variation of potential energy (ΔU_0). Indeed, the scission of a polyatomic molecule into two radicals results in changes to six internal vibrational modes, [i.e., one bond stretching (the reaction coordinate), one internal rotation and four rocking modes], three translation and three rotation modes with lower frequencies.[14] This transformation results in a substantial increase in entropy, while the ZPE decreases. We note Δg, the function that describes the net contribution of enthalpy and entropy variations in $\Delta G^{\ddagger}$ versus temperature, i.e.

$$\Delta \mathrm{g} = \int_T C_\mathrm{p}\,\mathrm{d}T - T\Delta S = \Delta H - T\Delta S \qquad (1)$$

As shown in Figure 1, Δg decreases along the reaction coordinate. Since $\Delta G^{\ddagger} = \Delta U + \Delta g$ (in this equation, $\Delta U = \Delta U_0 + \Delta E_{ZPE}$, where ΔE_{ZPE} is the zero-point energy difference between the reactant and the reaction intermediate), the free energy profile displays a maximum, the position of which is temperature dependent. This maximum (Figure 1) allows a TS to be identified in the generalized TST meaning. Since Δg becomes more negative with increasing temperature, the free energy barrier is more pronounced at higher temperatures. As a consequence, (i) transition states should be easier to locate at higher temperatures, (ii) TS looseness should decrease with temperature (which is qualitatively in agreement with other theoretical approaches previously cited), and (iii) the difference in free energy between the TS and dissociation products should increase with temperature.

Alternatively, transition states can be directly located on rate constant profiles, rather than free energy profiles. $\Delta G^{\ddagger}$ and the corresponding reaction intermediate rate constant $k^{\ddagger}$ are indeed equivalent, according to the expression

$$k^{\ddagger} = \kappa (c_0)^{1-m} \left(\frac{k_\mathrm{B} T}{h}\right) \exp\left(-\frac{\Delta G^{\ddagger}}{RT}\right) \qquad (2)$$

where k_B is the Boltzmann constant, h is the Planck constant, c_0 is a standard state concentration, m is the reactant molecularity of the reaction, and κ is the transmission coefficient accounting for tunneling along the reaction coordinate. Since $k^{\ddagger}$ and $\Delta G^{\ddagger}$ are inversely correlated, the TS at a given temperature can also be defined as the point along the reaction pathway which minimizes $k^{\ddagger}$.

2.3. Rate Constant Calculation. At the canonical level, $k^{\ddagger}$ can also be expressed as a function of the ratio of partition functions, corresponding to the different modes of motion of the reactant and reaction intermediate (note that when this reaction intermediate is the TS, $k^{\ddagger}$ is the reaction rate constant). In the case of the ethane dissociation reaction, assuming that ethane and any excited state along the reaction pathway are singly degenerate and neglecting the tunneling effect ($\kappa = 1$), $k^{\ddagger}$ can be approximated by

$$k^{\ddagger} = \frac{\sigma^{\mathrm{e}}}{\sigma^{\ddagger}} \left(\frac{k_\mathrm{B} T}{h}\right) \frac{(Q^{\mathrm{r}} Q^{\mathrm{v}})^{\ddagger}}{(Q^{\mathrm{r}} Q^{\mathrm{v}})^{\mathrm{e}}} \exp\left(-\frac{\Delta U}{RT}\right) \qquad (3)$$

where the superscript ‡ denotes the intermediate state and e refers to ethane. σ is the rotational symmetry number, i.e., $\sigma = 18$ for ethane. In this paper, we make the assumption that both separating fragments maintain a staggered D_{3d} orientation along the entire reaction pathway. The ratio $\sigma^{e}/\sigma^{\ddagger}$ therefore equals 1 in all cases. We are aware that such a hypothesis is rather drastic and may not be transferable to larger systems. Nevertheless, as previously mentioned in the specific case of ethane dissociation, the approximation seems acceptable for $r_{CC} < 4.5$ Å.[10] Q^{r} is the partition function for rigid rotation, and Q^{v} is the vibrational partition function for all of the internal degrees of freedom. We assume the harmonic approximation for all conserved modes, while transitional modes (except the reaction coordinate) are treated by a hindered rotor model. The partition function Q^{hr} for a hindered rotor is given by the general expression

$$Q^{\mathrm{hr}} = Q^{\mathrm{ho}} f = \frac{f}{1 - \mathrm{e}^{-u}} \qquad (4)$$

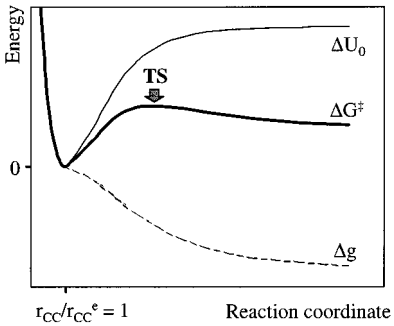

Figure 1. Comparison between potential (ΔU, corrected for ZPE) and free energy ($\Delta G^{\ddagger}$) variation along the reaction pathway, during a simple bond scission reaction. ΔU and $\Delta G^{\ddagger}$ are linked by the relation: $\Delta G^{\ddagger} = \Delta U + \Delta g$, where Δg is defined by eq 1). For dissociation processes, transition states (TS) can be accurately defined on $\Delta G^{\ddagger}$ profiles only.

where f is an interpolating function between the harmonic partition function Q^{ho} and the classical free rotor partition function Q^{fr}, and

$$u = \frac{h\omega}{k_{\mathrm{B}}T} \tag{5}$$

where ω is the vibrational frequency.

In this study, we use the interpolating function f suggested by Trulhar[15], i.e.

$$f = \tanh(Q^{\mathrm{fr}}u) \tag{6}$$

with

$$Q^{\mathrm{fr}} = \frac{2\pi\sqrt{2\pi I_{\mathrm{r}}k_{\mathrm{B}}T}}{\nu h} \tag{7}$$

where ν is the number of equivalent barrier minima ($\nu = 3$ for ethane) and I_{r} is the reduced moment of inertia. For ethane and reaction intermediates, I_{r} is given by

$$I_{\mathrm{r}} = \frac{3}{2}m_{\mathrm{H}}[r_{\mathrm{CH}}\sin(180^\circ - \gamma_{\mathrm{HCC}})]^2 \tag{8}$$

where m_{H} is the mass of the hydrogen atom, r_{CH} is the carbon−hydrogen bond distance and γ_{HCC} is the dihedral angle (see later discussion for geometry characterization).

After rearrangement, and considering eq 4, $k^{\ddagger}$ can be expressed by the following form:

$$k^{\ddagger} = \left(\frac{k_{\mathrm{B}}T}{h}\right)\left[\frac{(I_{\mathrm{a}}I_{\mathrm{b}}^2)^{\ddagger}}{(I_{\mathrm{a}}I_{\mathrm{b}}^2)^{\mathrm{e}}}\right]^{1/2}\frac{\{(\Pi_{i=3n-11}^{3n-7}f_{\mathrm{i}})(\Pi_{i=1}^{3n-7}(1-\mathrm{e}^{-u_i})^{-1})\}^{\ddagger}}{\{(\Pi_{\mathrm{i}=3n-11}^{3n-7}f_i)(\Pi_{i=1}^{3n-6}(1-\mathrm{e}^{-u_i})^{-1})\}^{\mathrm{e}}} \times \exp\left(-\frac{\Delta U}{RT}\right) \tag{9}$$

In this expression, I_{a} and I_{b} are the principle moments of inertia about the symmetry axis, which are parallel and perpendicular, respectively, to the axis passing through the two carbon atoms.[14] Note that since the D_{3d} symmetry is conserved, reaction intermediate structures are symmetric rotors, like ethane.

2.4. Activation Energy and Frequency Factor Assessment. Once the TS localized on $k^{\ddagger}$ profiles calculated at various temperatures, the activation energy (E_{a}) and the frequency factor (A) for the dissociation reaction were derived from an Arrhenius plot, according to

$$\ln(k_{\mathrm{TS}}^{\ddagger}) = \ln(\mathrm{A}) - E_{\mathrm{a}}/RT \tag{10}$$

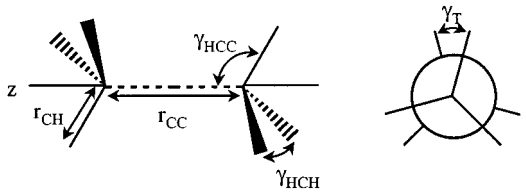

Figure 2. Structural parameters for the dissociation of ethane. r_{CC}, the bond distance between the two atoms of carbon, is the reaction coordinate. We assume that the two separating fragments have the same symmetrical axis (z).

TABLE 1: DFT B3:LYP 6-31G Simulation Results for the Reaction $C_2H_6 \rightarrow CH_3^{\bullet} + CH_3^{\bullet}$[a]**

r_{CC} (Å)	r_{CH} (Å)	γ_{HCH} (deg)	γ_{HCC} (deg)	γ_{T} (deg)	SCFE (hartree)
1.53[b]	1.0951	107.548	111.332	60.000	−79.838 749
2.00[b]	1.0877	112.651	106.066	60.000	−79.788 367
2.25	1.0851	114.811	103.494	59.859	−79.753 514
2.50	1.0832	116.436	101.086	60.147	−79.723 438
2.65	1.0827	117.602	99.009	60.041	−79.709 995
2.75	1.0822	118.263	97.606	61.537	−79.704 020
2.85	1.0821	118.794	96.320	61.329	−79.699 654
3.00	1.0817	119.335	94.639	61.055	−79.695 178
3.10	1.0817	119.593	93.745	61.503	−79.693 127
3.30	1.0816	119.869	91.928	62.293	−79.690 339
3.50	1.0817	119.970	91.077	62.950	−79.688 594
3.60	1.0818	119.993	90.166	61.811	−79.687 993
3.80	1.0818	119.994	90.038	62.470	−79.687 129
4.00	1.0820	120.000	89.948	62.460	−79.686 543
4.30	1.0820	120.000	89.948	65.147	−79.686 013
4.50	1.0820	120.000	89.948	65.147	−79.685 782
4.80	1.0820	120.000	89.948	65.147	−79.685 711
4.90	1.0820	120.000	89.948	65.147	−79.685 686
5.00	1.0820	120.000	89.948	65.147	−79.685 674
5.10	1.0820	120.000	89.948	65.147	−79.685 669
5.20	1.0820	120.000	89.948	65.147	−79.685 671
5.30	1.0820	120.000	89.948	65.147	−79.685 673
5.50	1.0820	120.000	89.948	65.147	−79.685 676
20.0	1.0820	120.000	90.074	64.102	−79.685 727

[a] Structural parameters (r_{CC}, r_{CH}, γ_{HCH}, γ_{HHC}, γ_{T}) refer to Figure 2. [b] Closed shell simulations.

where $k_{\mathrm{TS}}^{\ddagger}$ is the rate constant for the TS (i.e., $k_{\mathrm{TS}}^{\ddagger}$ is the minimum $k^{\ddagger}$ value at a given temperature).

3. Results and Discussions

Twenty-four geometries were selected and optimized along the reaction coordinate for C−C bond distances ranging from 1.53 Å (the coordinate at the reactant molecule) to 20 Å. Bond distance and angle parameters referred to in Figure 2 are reported in Table 1. This table also includes total electronic energies (SCFE, in hartree). Computed frequencies for all geometries are given in Table 2.

3.1. Geometry Properties. As the carbon−carbon bond is stretched, the separating fragments change from sp^3 to sp^2 hybridization. This leads to shorter carbon−hydrogen bond distances (reduced by approximately 1%), larger γ_{HCH} angles (up to 12%), and smaller γ_{HCC} angles (20%) [see Figure 3a−c]. The torsional angle γ_{T} in panel d does not display any significant variation until r_{CC} exceeds 2.8 Å. From this bond distance, the contribution of internal rotation to the total energy, which is responsible for the gauche configuration of ethane, becomes negligible. For higher carbon−carbon bond lengths, the random variation of γ_{T} indicates that the two fragments start to undergo free rotation.

As shown in Figure 3a−c, ab initio simulations predict exponential-like variations of r_{CH}, γ_{HCH}, and γ_{HCC} along the reaction coordinate r_{CC}, i.e., the carbon−carbon bond length. As a first approximation, this shape is qualitatively in agreement

TABLE 2: Frequency Modes and ZPE along r_{CC}[a]

	ZPE	transitional modes (cm^{-1})				conserved modes (cm^{-1})							
r_{CC} (Å)	(kcal/mol)	A_{1u}	A_{1g}	E_u	E_g	A_{2u}	A_{1g}	E_u	E_g	A_{2u}	A_{1g}	E_u	E_g
1.53[a]	47.0	315.2	1004.7	829.1	1226.6	1418.8	1440.5	1521.3	1516.6	3043.7	3042.4	3122.0	3097.9
exp.[b]	47.8	303	1016	822	1246	1438	1449	1526	1552	3061	3043	3140	3175
	n/a	289	995	822	1190	1379	1388	1469	1468	2896	2954	2985	2969
2.00[a]	44.1	154.8	−79.2	686.0	1000.3	1192.2	1194.7	1481.7	1477.7	3097.0	3095.7	3227.2	3222.4
2.25	43.0	110.8	−293.8	618.7	869.8	1066.8	1075.2	1465.8	1461.1	3115.3	3114.8	3264.5	3262.8
2.50	42.1	82.6	−371.7	552.7	745.0	954.0	964.1	1453.5	1449.4	3130.3	3129.9	3292.6	3291.4
2.65	40.9	70.8	−487.2	460.3	600.6	807.5	838.1	1442.5	1438.6	3133.2	3132.5	3301.8	3301.5
2.75	40.4	64.5	−418.5	407.3	518.1	729.9	765.4	1437.1	1433.4	3135.2	3134.3	3307.7	3306.6
2.85	39.9	59.3	−354.8	362.8	448.5	662.5	699.5	1433.0	1429.4	3136.4	3135.5	3311.6	3311.1
3.00	39.4	53.0	−275.2	308.1	364.5	586.4	620.0	1428.6	1425.3	3137.7	3136.8	3316.2	3315.5
3.10	39.2	49.6	−232.2	279.9	321.4	551.0	579.9	1426.6	1423.5	3137.6	3136.7	3317.2	3316.3
3.30	38.8	44.4	−167.4	234.2	254.9	509.3	526.4	1424.2	1421.6	3137.3	3136.8	3318.8	3318.1
3.50	38.6	40.8	−124.8	204.4	211.7	497.2	502.7	1423.2	1421.1	3136.2	3135.9	3318.0	3317.4
3.60	38.5	39.4	−109.4	194.4	197.4	495.6	496.7	1423.0	1421.1	3135.3	3134.8	3317.2	3316.3
3.80	38.4	37.3	−86.7	174.5	179.2	489.9	494.6	1422.4	1420.8	3134.7	3134.4	3316.6	3316.0
4.00	38.3	35.8	−72.0	162.4	168.7	487.5	495.0	1422.1	1420.8	3133.9	3133.6	3315.6	3315.1
4.30	38.3	34.3	−58.0	155.3	162.5	486.9	496.0	1422.2	1421.3	3132.3	3132.2	3314.2	3313.8
4.60	38.3	33.5	−45.1	149.3	156.4	486.2	495.3	1422.0	1421.2	3132.2	3132.0	3314.0	3313.6
4.80	38.3	33.1	−36.4	147.4	154.0	486.4	494.8	1421.9	1421.3	3132.1	3132.0	3314.0	3313.6
4.90	38.3	33.0	−32.8	147.3	153.6	486.5	494.9	1421.8	1421.3	3132.1	3132.0	3314.0	3313.6
5.00	38.3	32.9	−29.7	147.0	152.9	486.7	494.7	1421.8	1421.3	3132.1	3132.0	3314.0	3313.6
5.10	38.3	32.8	−26.8	146.5	152.3	486.9	494.6	1421.8	1421.3	3132.1	3132.0	3314.0	3313.6
5.20	38.3	32.7	−24.3	146.6	152.2	487.1	494.6	1421.7	1421.3	3132.1	3132.0	3314.0	3313.6
5.30	38.3	32.6	−22.3	146.5	152.0	487.3	494.5	1421.7	1421.3	3132.1	3132.0	3314.0	3313.6
5.50	38.3	32.5	−19.4	146.3	151.4	487.6	494.1	1421.7	1421.3	3132.1	3132.0	3314.0	3313.6
20.0	38.3	33.1	−18.9	147.8	152.0	491.6	491.8	1421.3	1421.0	3132.4	3132.2	3314.2	3313.9

[a] Closed shell simulations. [b] Experimental data: (top) harmonic and (bottom) fundamental frequencies given in ref 21.

with the assumption made by several authors (ref 7 and 8, among others), who interpolated geometrical property variations by means of a one-parameter function, as follows:

$$x = x^e + (x^m - x^e)e^{-\alpha(r_{CC} - r_{CC}^e)} \quad (11)$$

where x is a property (e.g., r_{CH}, γ_{HCC}, γ_T) with value x^e for ethane and x^m for a methyl radical and α is a parameter which controls the curvature of x along r_{CC}. Usually, it is assumed[7,8] that all geometrical properties vary along the reaction coordinate with the same α value (typically, $\alpha = 0.7-1$ Å^{-1}). In Figure 3, we used $\alpha = 1$, according to Wardlaw and Marcus[8]. Accordingly, a semilog plot of $(x - x^e)$ versus $(r_{CC} - r_{CC}^e)$ should generate a straight line, the slope of which gives α. However, in more detail our calculations are not fully consistent with this empirical model. First, as indicated by gray arrows in Figure 3, geometrical parameters do not reach their sp^2 configuration at the same coordinate: r_{CH} displays a very slight variation after $r_{CC} = 3$ Å, while sp^2 dihedral angles are attained at 3.4 Å for γ_{HCH} and 4.2 Å for γ_{HCC}. Therefore, each property should be characterized by a specific α value. Second, a detailed examination of data in Table 1 reveals that, at the level of theory assumed to optimize geometries, r_{CH} reaches a minimum value around $r_{CC} = 3.3$ Å, suggesting that umbrella opening first requires carbon−hydrogen bond shortening before it takes place completely. Such slight variations cannot be accounted for by eq 11.

Another interpolation function, suggested by Robertson et al.[16], has the form

$$x = x^e + (x^m - x^e)(1 - \tanh[\lambda_1 \Delta r_{CC}\{e^{\lambda_2 \Delta r_{CC}^3} + 1\}]) \quad (12)$$

where $\Delta r_{CC} = r_{CC} - r_{CC}^e$ and λ_1 and λ_2 are two fitting parameters which depend on the fitted property. As stated in ref 16, this type of function is more accurate than eq 11 for fitting geometrical properties, even when individual α values are used. Robertson et al. have calibrated λ_1 and λ_2 values (both relative to geometry, frequency modes and torsional barrier; see Table 10 of their paper) using data mostly obtained through generalized valence bond/configuration interaction (GVB/CI) simulations of ethane decomposition, using the 6-31G** basis set. Their model, also displayed in Figure 3, is in very good agreement with our data. This consistency validates geometries optimized by our approach. Analytical fits of our geometrical data were also performed using eq 12; corresponding parameters are provided in Table 3.

3.2. Potential Energies and Barrier to Internal Rotation. The D_{3d} potential energy path (ΔU_0, relative to equilibrium ethane) calculated at the UDFT B3:LYP 6-31G** level, according to the procedure described previously, is displayed in Figure 4. To compare our results with the GVB/CI 6-31G** profile published by Robertson et al.,[16] we show in Figure 4 the best interpolation function obtained by these authors to fit their data. The equation in question is a modified Morse function[19] with the following form:

$$\Delta U_0 = D[1 - \exp(-\beta \Delta r_{CC})]^2 \quad (13)$$

where $\beta = b_0 + \beta_1(\Delta r_{CC}) + \beta_2(\Delta r_{CC})^2 + \beta_3(\Delta r_{CC})^3$ and D is the reaction dissociation energy. There is a slight but significant difference between our results and those obtained by Robertson et al. Hence, we readjusted the free parameters (b_0, β_1, β_2, and β_3) in eq 13 in order to interpolate our data. Results are given in Table 4; the fit was completed with a regression coefficient (r^2) of 0.9998.

GVB/CI simulations lead to a lower dissociation energy (by about 2 kcal/mol) compared to UDFT B3:LYP calculations: $D_{\text{ref 18}} = 93.98$ kcal/mol and $D_{\text{this work}} = 95.80$ kcal/mol, respectively. The result we obtained is thus closer to the experimental value, estimated at 96.6−97.0 kcal/mol.[7,16] The analysis of SCFE for equilibrium ethane and dissociated structures (compare Table 1 of this paper with Table 2 in ref 16) indicates that, despite further CI calculations, the GVB approach leads to higher absolute SCFE than the UDFT B3:

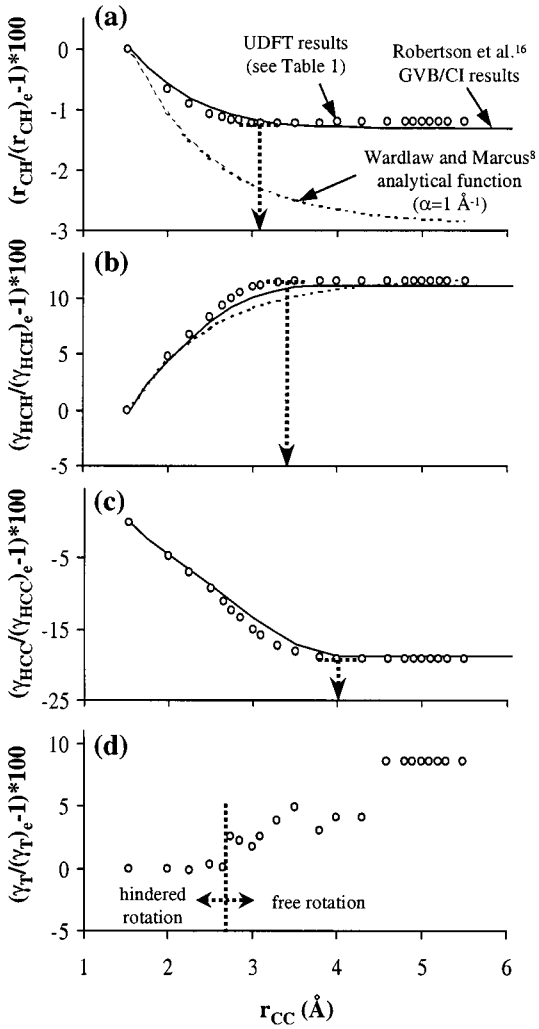

Figure 3. UDFT B3:LYP-predicted geometrical properties as a function of r_{CC}. Plotted parameters refer to Figure 2: (a) carbon−hydrogen bond length r_{CH}, dihedral angles (b) γ_{HCH} and (c) γ_{HHC}, and (d) torsional angle γ_T. $(r_{CH})_e$, $(\gamma_{HCH})_e$, $(\gamma_{HHC})_e$, and $(\gamma_T)_e$ are geometrical parameters in equilibrium ethane. Arrows indicate the coordinates at which values of sp^2 configuration are reached.

TABLE 3: Fitting Parameters of Eq 12 to Account for the Evolution of UDFT B3:LYP Geometrical Parameters Long the Reaction Pathway

	r_{CH} (Å)	γ_{HCH} (deg)	γ_{HCC} (deg)
x^e (r_{CC} = 1.53)	1.0951	107.548	111.332
x^m (r_{CC} = 5.50)	1.0820	120.000	89.948
λ_1 (Å^{-1})	0.6542	0.4428	0.2695
λ_2 (Å^{-3})	0.2554	0.1731	0.1445
r^2	0.9982	0.9996	0.9989

LYP calculation all along the reaction pathway (e.g., at the equilibrium ethane, $SCFE_{ref\ 16}$ = −79.551060 hartrees and $SCFE_{this\ work}$ = −79.838749 hartrees; at r_{CC} = 5 Å, $SCFE_{ref\ 16}$ = −79.401332 hartrees and $SCFE_{this\ work}$ = −79.685674 hartrees). It appears that the SCFE overestimation at the GVB/CI level is a little more pronounced at the equilibrium ethane, which explains the lower dissociation energy found by Robertson et al.

We did not perform ab initio treatments of both staggered (i.e., γ_T = 0 deg) and eclipsed (i.e., γ_T = 60 deg) conformations at each step along the reaction coordinate to derive potential energy barriers to internal rotation about the carbon−carbon bond. Instead, barrier heights (W) can be estimated from the following equation[14]:

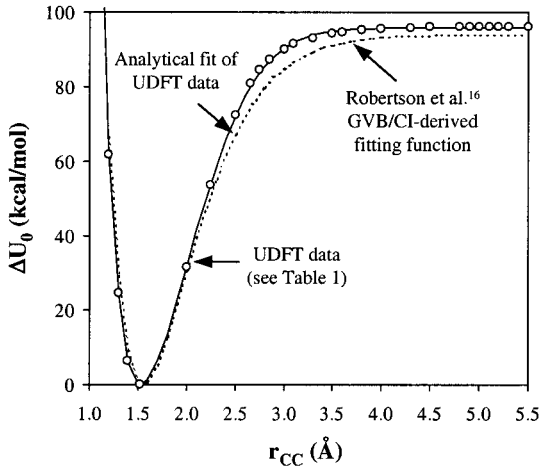

Figure 4. UDFT B3:LYP-predicted electronic energy profile for ethane dissociation.

TABLE 4: Fitting Parameters of Eq 13 to Account for the UDFT B3:LYP Potential Energy Profile

	Robertson et al.[16]	this work
r_{CC}^e (Å)	1.552	1.530
D (kcal/mol)	93.98	95.80
β_0 (Å^{-1})	1.80	1.73
β_1 (Å^{-2})	0.063 17	−0.000 24
β_2 (Å^{-3})	0.160 23	0.501 26
β_3 (Å^{-4})	−0.033 92	−0.123 48

$$W = 2I_r\left(\frac{2\pi\omega_{tor}}{\nu}\right)^2 \qquad (14)$$

where ω_{tor} is the vibrational frequency for internal rotation and ν = 3. Since the relative variations of I_r versus r_{CC} are low compared to ω_{tor}, the prediction of W along the reaction pathway mainly depends on the reliability of our simulations to predict variations of ω_{tor}. Using data given in Tables 1 and 2, we obtained a torsional barrier for equilibrium ethane at 2.97 kcal/mol, which is very close to the experimental value[3] of 2.89 kcal/mol. In Figure 5, we also show that W values as a function of r_{CC}, as calculated through eq 14, compare very well with theoretically derived data,[16] represented here by an interpolation function similar to eq 11 (with α = 3.00 Å^{-1}, x^m = 0, and x^e = 3.06 kcal/mol; see Table 10 in ref 16). This agreement validates indirectly geometrical parameters given in Table 1 and above all frequency modes for ω_{tor} (Table 2) at low bond stretching. We also confirm that the random variation of γ_T at r_{CC} > 2.8 Å, observed in Figure 1d, is consistent with the progressive disappearance of the barrier to internal rotation.

3.3. Vibrational Frequencies. Functions similar to eqs 11 and 12 were also assumed to interpolate the switching of frequencies along the reaction pathway.[7,8,16] Fitting parameters in eq 12, calibrated using our frequency data, are given in Table 5. As for geometries, only the exponential interpolation function appears to be qualitatively reasonable with regards to our calculations (see Figure 6), even though the use of individual α values rather than a global one would be more appropriate. Indeed, carbon−hydrogen stretching modes, which are related to the contraction of C−H bonds displayed in Figure 3a, have a slight variation after r_{CC} = 3 Å (nevertheless, as for r_{CH}, our simulations predict that these wavenumbers have a minimum value around r_{CC} = 3.3 Å). E_u and E_g bending modes in ethane, related to γ_{HCH}, are completely changed into one E′ mode at r_{CC} = 3.5 Å, while the transformation of A_{2u} and A_{1g} modes into one A_2'' mode requires more extensive carbon−carbon bond stretching to be completed. This last transposition is related to

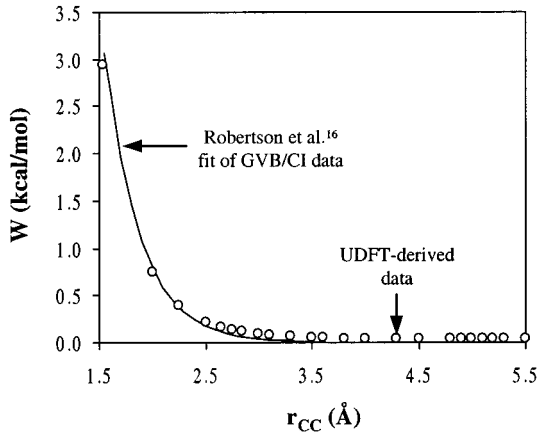

Figure 5. Predicted tortional energy barrier W along the reaction coordinate.

the decrease of γ_{HCC}, and a single exponential decrease law is not enough to account precisely for the apparent two-step process observed in Figure 6 for this mode.

Calculations performed by Robertson et al.[16] at the GVB/CI 6-31G** level are generally in good agreement with our data. As shown in Figure 4, while $r_{CC} \leq 3.5$ Å, eq 12 used with parameters calibrated by these authors fits perfectly the wavenumbers corresponding to the transitional modes. At larger bond distances, the interpolating function deviates from our predicted frequencies, which stabilize at higher values than those calculated by Robertson et al. This discrepancy is quantitatively important because the transitional modes control the variations of the ratio of vibrational partition functions ($Q_v^{\ddagger}/Q_v^{e}$ in eq 3) during the transition between harmonic oscillations and free rotations. Therefore, $k^{\ddagger}$ profiles generated from data provided in this paper and data given in ref 16 should expectedly diverge as the system progresses along the reaction coordinate.

Conserved frequency modes in Table 2 are not perfectly in accord with simulations performed by Robertson et al.;[16] however, the shapes of both ab initio data are very similar (Figure 6). A simple translation of the interpolation function to lower values (by switching x^e and x^m in eq 14 by about 100 cm^{-1}) would actually produce a good fit of wavenumbers reported in this paper. As a consequence, even though our data lead to lower zero-point energies compared to the data of ref 16, similar ZPE differences (i.e., previously noticed ΔE_{ZPE}) should be obtained by both simulations.

3.4. TS Location. Rate constants ($k^{\ddagger}$), as defined by eq 9, were computed at various temperatures, from 100 °C up to 2000 °C, along the reaction pathway. Each profile was then fitted by means of a specific cubic spline interpolant allowing for preserving the convex and concave regions implied by the data.[18] We have found it more reliable to interpolate rate constant profiles directly, rather than using functions like eqs 11 to 13, calibrated on data of Tables 1 and 2, to calculate $k^{\ddagger}$ at any temperature and any carbon−carbon bond distance. In the second approach, the uncertainty on $k^{\ddagger}$ is indeed always larger than in the method we used, due to the accumulation of numerical errors.

Transition states were then numerically localized at the minimum of $k^{\ddagger}$ profiles. Predicted TS coordinates along the reaction pathway are plotted as a function of temperature in Figure 7. To compare our results with literature data, the x-axis of this diagram is not set to $r_{CC}^{\ddagger}$, i.e., the carbon−carbon bond length at the TS, but to the distance $r_{CM}^{\ddagger}$, which separates the center of mass of the two methyl fragments (this reaction coordinate is indeed sometimes preferred to $r_{CC}^{\ddagger}$).

As expected, TS get tighter when temperature increases; however, $r_{CM}^{\ddagger}$ has a high-temperature limit that we estimate between 2.7 and 2.8 Å (this corresponds to $r_{CC}^{\ddagger} = 2.6-2.7$ Å). At low temperatures, the slight variations of $k^{\ddagger}$ in the region of its minimum value make TS localization uncertain.

In our approach, $k^{\ddagger}$ was evaluated in a canonical expression, neglecting the tunneling effect and excluding all possible relative orientations of the two methyl groups except the D_{3d} symmetry. Despite these strong simplifications, our calculations displayed in Figure 7 (plain curve) are in reasonable agreement with data previously published.[7,8,10,14,19] Note that all values plotted in this diagram were derived from theoretical treatments of the reaction, most of them on the basis of RRKM theory.[7,8,10,19] All models in this diagram are relatively consistent at high temperature (i.e., above 500°C). At lower temperatures, the predicted transition state locations are still in the range of literature data, but our model tends to diverge from them. This deviation becomes significant below 200°C, and can be explained by the simplifications we did in our approach, especially regarding the symmetry of the system.

Indeed, as the temperature decreases, the TS becomes looser. According to Klippenstein and Harding,[10] after a certain C−C distance (beyond 4 Å), the relative orientation of the two methyl fragments likely evolves from a face-to-face position to a structure where one fragment is perpendicular to the C−C axis and the other is parallel. Therefore, since we confined the symmetry of the system to D_{3d} regardless of the reaction coordinate, we did not estimate low temperature rate constants on the basis of the most likely TS. Another restriction to our approach is the use of a canonical rather than a microcanonical rate constant expression. As shown, for example by Wardlaw and Marcus,[8] the canonical expression may lead to an error of 20% in estimating the rate constant, compared to the microcanonical approach with energy and angular momentum resolution. However, this error does not appear to be temperature dependent; therefore, it has probably not a major contribution to the deviation observed in Figure 7.

3.5. "Thermodynamic" Interpretation. The free energy of activation has been defined previously in eq 2. It is interesting to investigate from a "thermodynamic" point of view the factors that control the temperature dependence of TS location. For this, we rewrite $\Delta G^{\ddagger}$ as the sum of energies associated with SCFE, ZPE, enthalpy and entropy transformations along the reaction pathway

$$\Delta G^{\ddagger} = \Delta H^{\ddagger} - T\Delta S^{\ddagger} = \epsilon_{SCFE} + \epsilon_{ZPE} + \epsilon_{H} + \epsilon_{S} \quad (15)$$

where $\epsilon_{SCFE} = \Delta U_0$, $\epsilon_{ZPE} = \Delta E_{ZPE}$, $\epsilon_H = \Delta H_T^{\ddagger}$, and $\epsilon_S = -T\Delta S^{\ddagger}$. $\Delta H^{\ddagger}$ is the enthalpy of activation (i.e., $\Delta H^{\ddagger} = \Delta U_0 + \Delta E_{ZPE} + \Delta H_T^{\ddagger}$), $\Delta H_T^{\ddagger}$ is the thermal contribution to $\Delta H^{\ddagger}$, and $\Delta S^{\ddagger}$ is the entropy of activation. Thermodynamic functions $\Delta H_T^{\ddagger}$ and $\Delta S^{\ddagger}$ can be evaluated from partition functions for all degrees of freedom[14] (i.e., transitional, rotational and vibrational), along the reaction pathway.

Diagrams displayed in Figure 8 show contributing energies ϵ_{SCFE}, ϵ_{ZPE}, ϵ_H and ϵ_S versus r_{CC}, at two different temperatures (300 and 1500 °C). These diagrams, based on data given in Tables 1 and 2, clearly reveal the importance of the interplay between ΔU_0 and $\Delta S^{\ddagger}$ on the shape of $\Delta G^{\ddagger}$ profiles and, therefore, on TS location. Indeed, whatever the temperature, ΔE_{ZPE} and $\Delta H_T^{\ddagger}$ both have low contributions, which partly compensate each other since $\epsilon_{ZPE} < 0$ and $\epsilon_H > 0$. Quantitatively, $\Delta G^{\ddagger}$ is mostly accounted for by ΔU_0 at low temperature and by both ΔU_0 and the energy associated with $\Delta S^{\ddagger}$ at high

TABLE 5: Fitting Parameters of Eq 12 to Account for the Evolution of UDFT B3:LYP Vibrational Frequencies Long the Reaction Pathway

	transitional modes modes (cm^{-1})			conserved modes (cm^{-1})							
	A_{1u}	E_u	E_g	A_{2u}	A_{1g}	E_u	E_g	A_{2u}	A_{1g}	E_u	E_g
$\omega^e(r_{CC} = 1.53)$	315.2	829.1	1226.6	1418.8	1440.5	1521.3	1516.6	3043.7	3042.4	3122	3097.9
$\omega^m(r_{CC} = 5.50)$	32.5	146.3	151.4	487.6	494.1	1421.7	1421.3	3132.1	3132	3314	3313.6
λ_1 ($Å^{-1}$)	0.6140	0.2550	0.2608	0.2634	0.2717	0.4238	0.4343	0.6805	0.6753	0.6318	0.6748
λ_2 ($Å^{-3}$)	−0.0867	0.1412	0.1960	0.3353	0.2654	0.1649	0.2126	0.6481	0.6539	0.2416	0.1986
r^2	0.9974	0.9931	0.9952	0.9981	0.9988	0.9988	0.9991	0.9904	0.9929	0.9988	0.9991

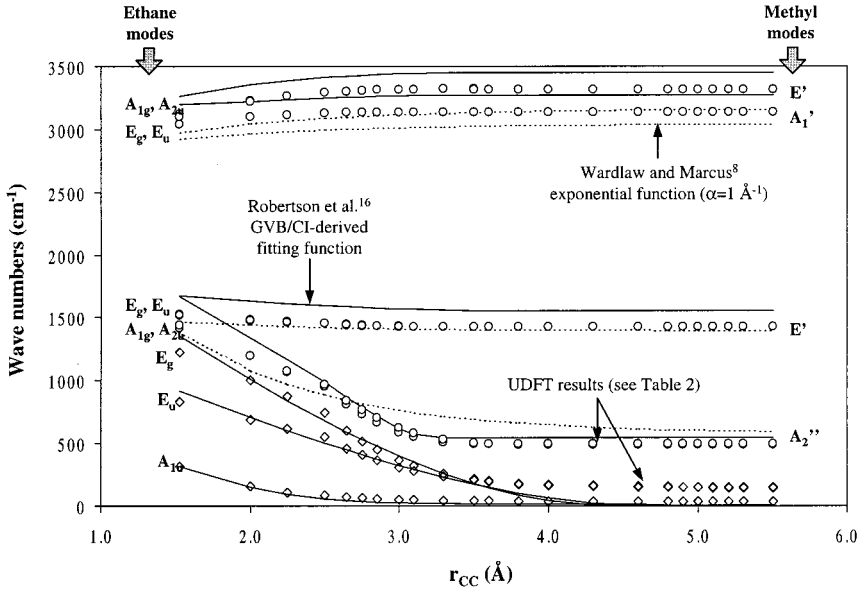

Figure 6. Comparison between UDFT B3:LYP-derived frequencies and interpolation functions given in the literature.

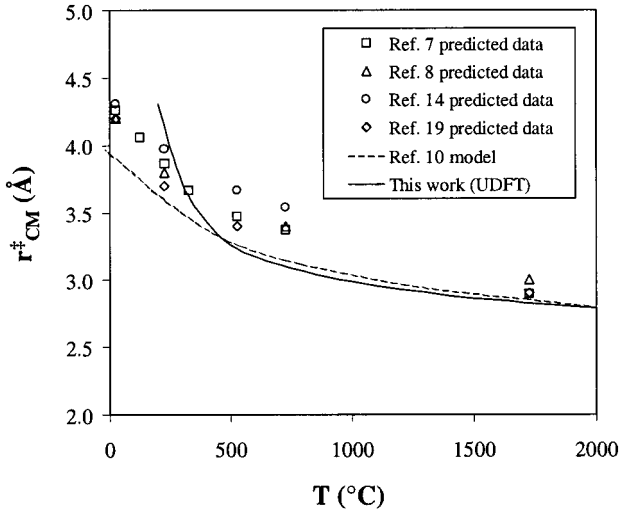

Figure 7. Coordinate of the transition state for ethane dissociation as a function of the temperature.

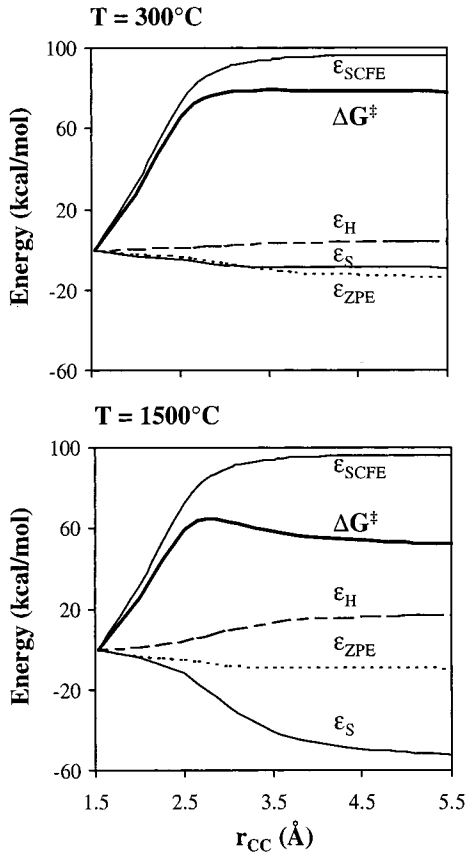

Figure 8. Contributing parameters to the free energy of activation, as a function of r_{CC}.

temperature. More precisely, when the rise of ϵ_{SCFE} is higher than the decrease of ϵ_S, i.e., when $|\partial\epsilon_{SCFE} > \partial r_{CC}| > |\partial\epsilon_S > \partial r_{CC}|$, then $\Delta G^‡$ increases. Inversely, $\Delta G^‡$ is reduced when $|\partial\epsilon_{SCFE} > \partial r_{CC}| < |\partial\epsilon_S > \partial r_{CC}|$. Accordingly, the coordinate at which $|\partial\epsilon_{SCFE} > \partial r_{CC}| = |\partial\epsilon_{SCFE} > \partial r_{CC}|$ is the approximate location of the TS (especially at high temperature). This interplay between ΔU_0 and $\Delta S^‡$ is illustrated in Figure 9. The curves plotted in this diagram have been evaluated from interpolation and numerical derivation of data displayed in Figure 8. Since ϵ_{SCFE} does not depend on temperature, we clearly see Figure 9 that the variation of $r^‡_{CC}$ with T is due to the temperature dependence of $|\partial\epsilon_S > \partial r_{CC}|$, which results from the positive correlation between $\Delta S^‡$ and T. This figure emphasizes also the importance of the curvature of ϵ_{SCFE}, which controls the magnitude of $r^‡_{CC}$ variations versus T.

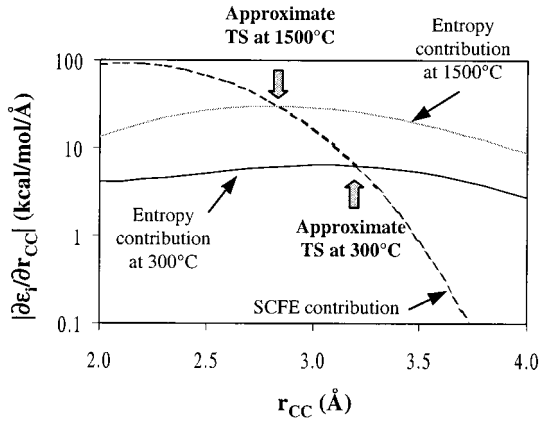

Figure 9. Illustration of the interplay between ϵ_{SCFE} and ϵ_S, controlling the temperature dependence of TS position along the reaction coordinate.

TABLE 6: Predicted Transition State Location along the Reaction Coordinate and Corresponding Dissociation and Recombination Rate Constants, at Various Temperatures and 1 atm

			dissociation		recombination
T (°C)	$r^{\ddagger}_{CC}$ (Å)	$r^{\ddagger}_{CM}$ (Å)	ln $k^{\ddagger}_{TS}$ (s^{-1})	ln K_{eq} ($cm^3\ mol^{-1}$)	ln $k^{\ddagger}_{TS,-1}$ ($cm^3\ mol^{-1}\ s^{-1}$)
300	3.611	3.612	−39.442	−69.578	30.136
500	3.218	3.237	−18.970	−48.836	29.866
700	3.078	3.108	−7.104	−36.606	29.502
900	2.978	3.015	0.631	−28.566	29.197
1100	2.905	2.948	6.043	−22.895	28.938
1300	2.849	2.896	10.026	−18.691	28.717
1500	2.803	2.855	13.070	−15.459	28.529

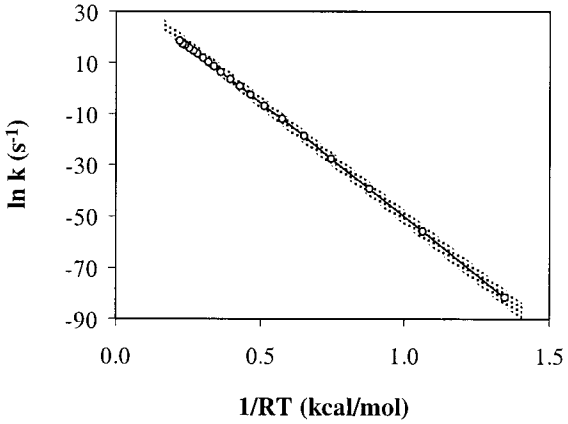

Figure 10. UDFT B3:LYP-predicted dissociation rate constants in an Arrhenius plot. The gray shape indicates the variability of data available in the literature (after ref 20).

3.6. Dissociation and Recombination Rate Constants. Ab initio predicted rate constants $k^{\ddagger}_{TS}$ for ethane dissociation are given in Table 6. In the temperature range 100−2000 °C, calculated rate constants display a quasi-linear correlation in an Arrhenius plot ($r^2 = 0.9999$), as shown in Figure 10. In this diagram, the gray shape represents the range of variation of $k^{\ddagger}_{TS}$ according to experimental and theoretical activation parameters available in the literature (we used data compiled by Allara and Shaw[20]). The very good agreement between ab initio results and these data validates the approach suggested in this paper. We derived a frequency factor at $10^{16.7}\ s^{-1}$ (for $T = 100-2000$ °C), in the range of expected values (i.e., $10^{16.3}$ to $10^{17.4}\ s^{-1}$). The corresponding activation energy was determined at 88.8 kcal/mol, which is consistent with literature data (i.e., between 86 and 91 kcal/mol).

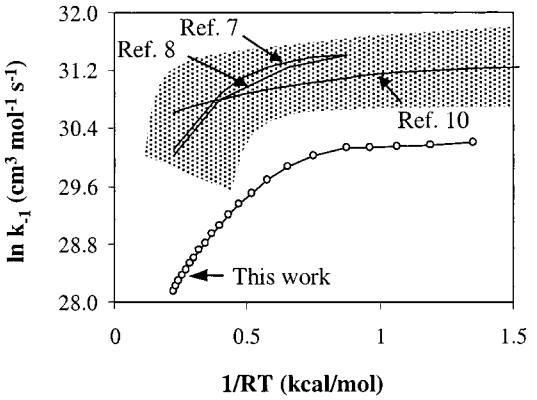

Figure 11. UDFT B3:LYP-predicted rate constants for methyl recombination in an Arrhenius plot. The gray shape corresponds to experimental and theoretically derived data given in ref 8.

It is of interest to verify also the reliability of our method for predicting rate constants for the backward reaction, i.e., methyl recombination. Assuming that at a given temperature recombination and decomposition processes lead the same TS, the recombination rate constant $k^{\ddagger}_{TS,-1}$ at the TS coordinate is related to the dissociation rate constant through the equilibrium constant K_{eq} (in concentration units) by[14]

$$k^{\ddagger}_{TS,-1} = \frac{k^{\ddagger}_{TS}}{K_{eq}} \tag{16}$$

Quantum mechanics simulations of equilibrium ethane and methyl radical were performed to determine K_{eq}. Recombination rate constants were then calculated at various temperatures according to eq 16. Results are given in Table 6 and plotted in an Arrhenius diagram in Figure 11. In this figure, the gray shape corresponds to theoretical and experimental data from various papers referenced by Wardlaw and Marcus.[8]

Ab initio calculations are not exactly consistent with methyl recombination rate constants suggested in the literature; however, they are in the same order of magnitude. Predicted $k^{\ddagger}_{TS,-1}$ values are indeed a bit underestimated compared to other calculations. This underestimation is surprising, since the use of a canonical expression to calculate rate constants leads to overestimated $k^{\ddagger}_{TS,-1}$ values compared to microcanonical models.[8] This discrepancy is probably due to compensations between the various uncertainties implied by our hypotheses.

Qualitatively, our approach accounts correctly for the negative temperature dependence of $k^{\ddagger}_{TS,-1}$, displayed in Figure 11, but this result is not unexpected. This specific shape, abundantly discussed in previous works,[5−9,19,21] arises from the fact that, due to the temperature dependence of TS location, the variations in $k^{\ddagger}_{TS}$ as a function of T have a higher magnitude that variations in K_{eq}. Consequently, the ratio $k^{\ddagger}_{TS}/K_{eq}$ (and therefore $k^{\ddagger}_{TS,-1}$) increases when T decreases and decreases when T increases. Thermodynamically, this result is accounted for by a positive correlation between the temperature and the recombination free energy of activation, while $\Delta G^{\ddagger}$ for the decomposition reaction exhibits negative temperature dependence.

4. Summary

In this study, a canonical transition state theory was applied to determine ethane dissociation rate constants. The approach we tested was based on ab initio simulations of the reaction at the UDFT B3:LYP level of theory, using the 6-31G** basis set. These calculations provided geometrical parameters, vibra-

tional frequencies and potential energies along the reaction pathway, i.e., the carbon−carbon bond distance. Corresponding rate constants were then calculated at various temperatures, and transition states were localized at the minimum of each $k^{\ddagger}$ profile. The methodology presented in this paper is only an application of already existing quantum mechanical tools to a specific process, which cannot be treated by standard TS search methods available in most current software packages. There is no precise description of the physics of dissociation and recombination reaction, as done in other publications tackling this subject in details. Our aim is to assess dissociation rate constants through a method that can be transferred to other systems. Because this method has been established to be generalized, it cannot lead the same level of accuracy than that obtained through more sophisticated but focused models. In the case of ethane, major uncertainties are due to the assumption of a D_{3d} symmetry system whatever the reaction coordinate, especially at large C−C bond distance, and also to the use of a canonical expression to calculate rate constants. Both hypotheses imply that our approach is probably weak for predicting rate constants at low temperatures (i.e., at least below 200 °C).

Despite such drastic restrictions, this first validation on ethane yields satisfactory results: the predicted temperature dependence of TS location is in agreement with other theoretically derived data, and the final absolute activation parameters are consistent with values available in the literature. Our method is more accurate at high temperature and may offer a reasonable first estimation of dissociation kinetic parameters in hydrocarbon systems. Rate constants for methyl recombination cannot be precisely predicted; however, their order of magnitude and their specific temperature dependence may be assessed. Unfortunately, the fair consistency between our calculations and other methyl recombination models is probably fortuitous, and cannot be guaranteed in other systems.

Acknowledgment. We gratefully acknowledge Dr. Paul Kralert and an anonymous reviewer for their very helpful comments and advises on his paper.

References and Notes

(1) Glasstone, S.; Laidler, K. J.; Eyring, H. *The Theory of Rate Processes*; McGraw-Hill: New York, 1941.

(2) Wright, J. R. *Jaguar User's Guide*; Schrödinger, Inc.: Portland, OR, 1998.

(3) Levine, I. N. *Quantum Chemistry*, 5th ed.; Prentice-Hall: Upper Saddle River, NJ, 2000.

(4) Golden, D. M. *J. Phys. Chem.* **1979**, *83*, 108.

(5) Garret, B. C.; Trulhar, D. G. *J. Phys. Chem.* **1979**, *70*, 1593.

(6) Gilbert, R. G.; Smith, S. C. *Theory of Unimolecular and Recombination Reactions*; Blackwell Scientific Publications: Cambridge, MA, 1990.

(7) Pesa, M.; Pilling, M. J.; Robertson, S. H.; Wardlaw, D. M. *J. Phys. Chem. A* **1998**, *102*, 8526.

(8) Wardlaw, D. M.; Marcus, R. A. *J. Phys. Chem.* **1986**, *90*, 5383.

(9) Wong, W. H.; Marcus, R. A. *J. Phys. Chem.* **1971**, *55*, 5625.

(10) Klippenstein, S. J.; Harding, L. B. *J. Phys. Chem. A* **1999**, *103*, 9388.

(11) Marcus, R. A. *J. Chem. Phys.* **1952**, *20*, 359.

(12) *JAGUAR*, version 4.0, release 13 ed.; Schrödinger, Inc.: Portland, OR, 1998.

(13) Kohn, W.; Sham, L. J. *Phys. Rev. A* **1965**, *140*, 1133.

(14) Benson, S. W. *Thermochemical Kinetics*, 2nd ed.; J. Wiley & Sons: New York, 1976.

(15) Trulhar, D. G. *J. Comput. Chem.* **1990**, *17*, 1064.

(16) Robertson, S. H.; Wardlaw, D. M.; Hirst, D. M. *J. Chem. Phys.* **1993**, *99*, 7748.

(17) Hase, W. L.; Mondro, S. L.; Duchovic, R. J.; Hirst, D. M. *J. Am. Chem. Soc.* **1987**, *109*, 2916.

(18) Irvine, L. D.; Marin, S. P.; Smith, P. W. *Constructive Approximation* **1986**, *2*, 129. We used the algorithm available in the IMSL Math/Library (i.e., CSCON subroutine).

(19) Smith, S. C. *J. Phys. Chem.* **1993**, *97*, 7034.

(20) Allara, D. L.; Shaw, R. *J. Phys. Chem. Ref. Data* **1980**, *9*, 523.

(21) Melissas, V. S.; Truhlar, D. G. *J. Phys. Chem.* **1994**, *98*, 875.